First-principles calculation of phase equilibria in the aluminum lithium system

M. Sluiter* and D. de Fontaine
Department of Materials Science and Mineral Engineering, University of California, Berkeley, Berkeley, California 94720

X. Q. Guo, R. Podloucky,† and A. J. Freeman
Department of Physics and Astronomy, Northwestern University, Evanston, Illinois 60207
(Received 14 November 1988; revised manuscript received 11 December 1989)

Volume-dependent total energies of Al, Li, and various intermetallic Al-Li compounds have been calculated by the first-principles full-potential linearized augmented-plane-wave (FLAPW) method. These values have been used to calculate Al-Li phase diagrams according to the cluster variation method in the tetrahedron approximation. Methods for performing lattice-parameter optimization and for including relaxation effects are presented. Truly first-principles-based phase diagrams for solid phases computed without any fitting parameters or empirical formulas are shown to exhibit a remarkable agreement with experimental data. Subsequently, some empirical equations for the free energy of the liquid and the vibrational entropy have been added to the first-principles results and striking similarities with experimental phase diagrams were obtained. Special attention has been paid to the metastable Al_3Li phase and to the mechanical properties of Al-rich Al-Li alloys. Furthermore, the influence of relaxation and vibrational entropy are discussed.

I. INTRODUCTION

The calculation of (metastable) equilibria in the aluminum-lithium system has attracted considerable attention[1–6] because of the technical importance of Al_3Li precipitation hardening in Al-rich Al-Li alloys. First-principles approaches for the study of phase transformations are of special interest in the case of the Al-Li system because of the difficulties encountered with experimental determinations of the metastable phase boundaries. Furthermore, first-principles approaches have the advantage of providing a deeper understanding of the underlying physics. In this paper the term "first-principles" will be used for results that do not in any fashion rely on experimentally determined quantities. The most interesting solid part of the phase diagram, up to the melting temperatures, is obtained from first-principles electronic-structure calculations without any experimental data. However, in order to get a complete phase diagram, which includes the liquid phase and accounts for vibrational entropy effects, we have to rely on empirical data. In the last decade the prediction of structural stabilities of phases at 0 K has become possible through accurate electronic-band-structure computations[7] based on local density functional theory.[8] Only recently have first-principles approaches become feasible for computation of phase stability away from 0 K,and various schemes, such as outlined in Refs. 9 and 10, are yielding increasingly realistic results. In this paper an approach involving highly precise full-potential linearized augmented-plane-wave (FLAPW)[11] total-energy computations will be applied and discussed.

The basic problem of all these approaches (including our own) is to derive parameters for a proper statistical treatment. In this paper we follow the concept of Connolly and Williams[12] to obtain many-body cluster interactions from volume-dependent total energies of a series of ordered compounds. The Connolly-Williams method has gained notable importance.[10,13] We refer to Ref. 14 for a preliminary discussion of its underlying assumptions. Here the cluster interactions are introduced in a statistical model, in this case in the tetrahedron cluster variation method (CVM), for calculating configurational free energies. The configurational free energies of various phases can be complemented with free-energy contributions from other sources[13,15] such as vibrational or relaxation effects to yield total free energies, which in turn are then used to obtain a phase diagram. In addition, a straightforward method for lattice-parameter optimization within the formulation of the CVM and an approximate treatment of relaxation effects will be presented.

II. GENERAL METHOD

In the Al-Li phase diagram (Fig. 1), as in many other systems, one may distinguish (a) terminal solid solutions, here designated as α (fcc) and β (bcc); (b) ordered superstructures, designated $\alpha_1,\alpha_2,\ldots$, if they are superstructures of the fcc lattice, and $\beta_1,\beta_2,\ldots$, if they are superstructures of the bcc lattice; and (c) additional intermetallic phases which are neither superstructures of fcc nor bcc, but which have very narrow ranges of stability. Two such "interloper" phases exist in the Al-Li system (see Ref. 16): Al_4Li_9 ($mC26$ Pearson symbol, $B2/m$ space group), and Al_2Li_3 ($h\bar{R}5$ Pearson symbol, $\bar{R}3m$ space group). In this study only the parent fcc and bcc lattices and their superstructures will be considered. Ignoring the two interloper phases has no consequences for the

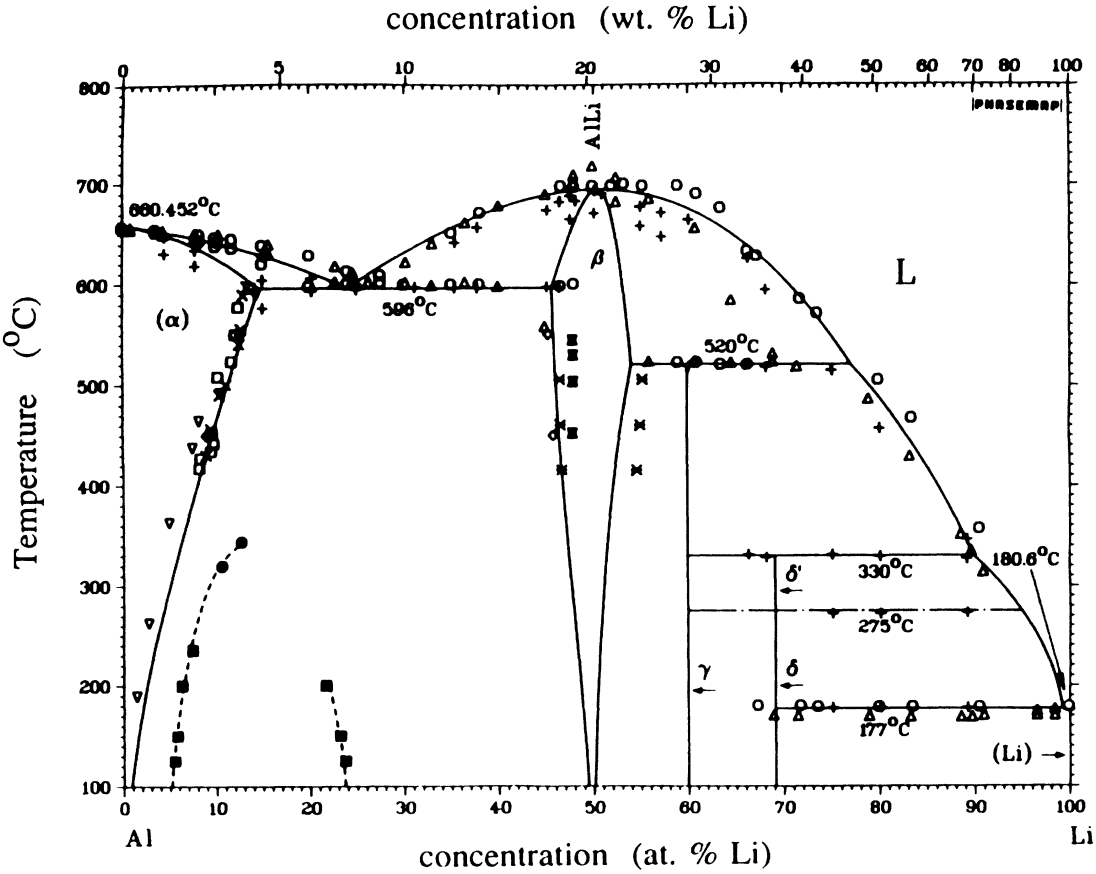

FIG. 1. Experimental Al-Li phase diagram, from Ref. 4.

technologically important Al-rich side of the phase diagram.

Volume-dependent total energies of fcc and bcc superstructures were computed with the FLAPW method. These total energies were used to obtain effective cluster interactions, by means of the Connolly-Williams method. In this method it is assumed that the cohesive energies can be expressed as the sum of the products of cluster interactions and cluster correlation functions.[12] Because the cluster correlation functions of perfectly ordered compounds are solely determined by the crystal structure in question, cluster interactions can be obtained provided that total energies for a set of ordered compounds are known. The cluster interactions are given by the product of the inverse cluster correlation matrix and the total-energy vector. The interactions, in turn, were employed in a statistical method so as to provide insight into phase stability at nonzero temperatures. The statistical method used in the present calculation is the CVM, whereby the free energy is expressed as a function of cluster correlations. Only the simplest tetrahedron cluster approximation will be used:[10,13] In the fcc lattice, the basic cluster is thus the regular tetrahedron made up of nearest-neighbor distances only; in the bcc it is the irregular tetrahedron containing both first- and second-neighbor distances. The ordered structures to be considered are thus limited to those which can be stabilized, for fcc superstructures, by first-neighbor pair interactions only, and for bcc, by first and second pair interactions. For the former we have, explicitly, the $L1_2$ (α_1,Al_3Li), $L1_0$ (α_2,AlLi), and $L1_2$ (α_3,$AlLi_3$) structures; for the latter, $D0_3$ (β_1,Al_3Li), $B2$ (β_2,AlLi), $B32$ (β_3,AlLi), and $D0_3$ (β_4,$AlLi_3$). Fortunately, in the Al-Li system, ordered superstructures of more complicated type are not found, so that the tetrahedron approximation, in both fcc and bcc, should be suitable. As very recently shown, the combination of first-principles electronic-structure calculations and the CVM via the Connolly-Williams method appears to be rather promising also for other systems.[10,12,13] A detailed examination of the validity of the tetrahedron approximation and of the Connolly-Williams method itself in the Al-Li system is currently under way.[17] In that study 16 superstructures on the fcc lattice will be employed for computation of all interactions included in the tetrahedron-octahedron cluster. The applicability of the CWM will be verified by studying a hierarchy of CWM approximations, rather than by showing that within a certain approximation the cluster interactions decrease with increasing cluster size.[10] This latter procedure was shown to be an invalid criterion.[14]

In a previous study[18] an attempt was made to derive phase stabilities or related quantities directly from the Schrödinger equation without any additional assumptions

such as the breaking up of the total energy in terms of cluster interactions as used in the present study. In the work of Podloucky *et al.*,[18] 8-atom fcc supercells (or 256 configurations) were used to study the Al-rich side of the phase diagram by calculating phase stabilities defining phases as a particular mixture of supercells. Because of this rather small number of configurations, one cannot expect this approach to yield quantitatively useful results.

The study presented in this paper differs radically from a previous study[18] in that here we are not interested in relative occurrences of fcc supercell configurations, but rather in the equilibrium thermodynamic properties and the complete phase diagram pertaining to fcc- and bcc-based superstructures. A comparison of Fig. 3 in Ref. 18 and the phase diagrams in this paper is therefore not possible.

A. Total-energy computations

Calculation of the phase diagram of a binary alloy with the Connolly-Williams method[12] requires volume-dependent total energies of a set of compounds, that is, superstructures of a given lattice (as will be discussed in Sec. II D). Sometimes the energy difference between the different crystal structures of a given compound is very small. Especially in the Al-Li system, because of the presence of the metastable Al_3Li-$L1_2$ phase, the total energy must be computed very accurately. Therefore, to get the correct result, the first-principles total-energy calculation should be done as accurately as possible. For this reason we use the highly precise all-electron FLAPW method[11] in which one makes no approximations to the shape of the one-electron potential or the charge density.

The total energy can be calculated within the framework of the local-density approximation in which Hedin and Lundqvist's exchange and correlation potential is chosen.[19] The total energy per unit cell is then given by

$$E_{\rm tot}=\sum_i \varepsilon_i-\tfrac{1}{2}\int_\Omega n(r)V_c(r)d^3r - \int_\Omega n(r)[V_{xc}(r)-\varepsilon_{xc}(r)]d^3r-\tfrac{1}{2}\sum_\nu Z_\nu V_M(r_\nu)\ , \tag{1}$$

where ε_i is the eigenvalue obtained by solving the Kohn-Sham equation, Z_ν and $n(r)$ are nuclear charge and charge density, and $V_c(r)$, $V_{xc}(r)$, and $V_M(r)$ are Coulomb, exchange-correlation, and Madelung potentials, and ε_{xc} is the exchange-correlation energy.

It needs to be emphasized that in the FLAPW method, there are no uncontrolled numerical parameters in the calculation. The only approximation in this method is the local-density approximation. In our computation the potential and charge density are expanded in spherical harmonics up to $l=8$ inside the spheres and the plane waves go up to $|G|=7.5$ a.u. in the interstitial. The number of basis functions is about 50 per atom in all cases. To check the accuracy we also increased the values of the expansion parameters and found that the difference due to the change of these parameters is very small (<0.1 mRy), which means that our choice of the parameters is sufficient for the desired accuracy.

The most sensitive parameter for the calculation of the absolute total energy is the number of **k** points in an irreducible wedge of the Brillouin zone (IBZ) used for integrations in the reciprocal space. This is because we use the analytic linearized tetrahedron method[20] in the construction of the charge density and total energy, which depends critically on the Fermi-surface topology. However, note that the error in the total energy in the linearized energy tetrahedron method scales as $N_{\mathbf{k}}^{-2/3}$ ($N_{\mathbf{k}}$ is the number of **k** points).[11] Thus, for each structure of the intermetallic compound, we calculated the total energy for a series of **k** points, say, 30, 60, 90, 150, 200, and 250, depending on the structure concerned, and we obtained the total energies for an infinite number of **k** points by extrapolation.

B. Relative energies and free energies

The FLAPW method provides total energies as a function of molar volume. By minimizing the total energy of a given phase with respect to volume, the equilibrium total energy $E_{\rm tot}^0$ and the equilibrium volume V_0 of a given phase are found. Moreover, the curvature of the total energy with volume is related to the bulk modulus:

$$B=V_0\left[\frac{\partial^2 E_{\rm tot}}{\partial V^2}\right]_{V=V_0}\ . \tag{2}$$

The cohesive energy $E_{\rm coh}$ of a given phase is commonly defined as the total energy of that particular phase minus the total energy of the constituent atoms at infinite separation. The cohesive energy is thus a measure of the cohesion of the atoms and should therefore be comparable to the sublimation energy. For the study of phase equilibria, the cohesive energy is more descriptive than the total energy, since the latter includes a large contribution from electronic states that do not play a role in bonding. One can use the cohesive energy instead of the total energy because these energies only differ by a linear function of composition. In the following we will, therefore, use the cohesive energy where applicable.

In this paper the formation energy $E_{\rm form}$ of a given phase ψ_i is given by the energy which would be generated if that phase were formed from the pure elements with the fcc structure, formally,

$$E_{\rm form}^{\psi_i}=E_{\rm coh}^{\psi_i}-(1-c)E_{\rm coh}^{\text{Al-fcc}}-cE_{\rm coh}^{\text{Li-fcc}}\ , \tag{3}$$

where $c=c_{\rm Li}$ is the lithium concentration in the ψ_i phase (the aluminum concentration is given by $c_{\rm Al}=1-c$). The formation energy is introduced in order to facilitate a comparison of the stability of phases, as the cohesive and total energies contain large contributions that are irrelevant for the study of phase equilibria.

For each phase i and parent lattice ψ, the Helmholtz free energy F can be expressed as a sum of two terms:

$$F^{\psi_i}(V)=F_{\rm lin}^{\psi}+F_{\rm mix}^{\psi_i}(V)\ , \tag{4}$$

where $F_{\rm mix}$ is the free energy of mixing, and where

$$F^{\psi}_{\rm lin}=(1-c)F^{{\rm Al},\psi}+cF^{{\rm Li},\psi}\ , \tag{5}$$

where $F^{\rm Al}, F^{\rm Li}$ are free energies of the pure components with fcc or bcc structure, at their respective equilibrium volumes. Each pure component free energy (F^{I}) is assumed to contain a cohesive and a vibrational contribution:

$$F^{I,\psi}=F^{I,\psi}_{\rm coh}+F^{I,\psi}_{\rm vib}\ ,$$

where $F^{I,\psi}_{\rm coh}$ is the cohesive free energy, and $F^{I,\psi}_{\rm vib}$ is the vibrational free energy. Since the temperatures of interest for alloying are much lower than the Fermi temperature, the cohesive free energy is virtually temperature independent. Hence $F^{I,\psi}_{\rm coh}$ can be replaced by the cohesive energy at 0 K, $E^{I,\psi}_{\rm coh}$. The vibrational free energy vanishes at 0 K except for a minute fraction due to the zero point motion. In this paper we ignore the zero point motion and assume that the vibrational entropy $S^{I,\psi}_{\rm vib}$ is temperature independent. Hence the pure component free energy can be expressed as

$$F^{I,\psi}=E^{I,\psi}_{\rm coh}-TS^{I,\psi}_{\rm vib}\ . \tag{6}$$

A comparison of the stability of the bcc and fcc lattices is now possible provided that the energy difference $\Delta E^{\rm fcc\text{-}bcc}=E^{\rm fcc}_{\rm coh}-E^{\rm bcc}_{\rm coh}$ and the entropy difference $\Delta S^{fcc\text{-}bcc}_{\rm vib}=S^{\rm fcc}_{\rm vib}-S^{\rm bcc}_{\rm vib}$ are known. Vibrational entropy will be included by subtracting the term $TS^{\psi}_{\rm vib}(c)$ from the configurational free energy. Note that we assume that the vibrational entropy is a function of composition and parent lattice type ψ, but not dependent on the type of order.

The free energy of mixing, $F^{\psi}_{\rm mix}=E^{\psi}_{\rm mix}-TS^{\psi}_{\rm mix}$, will depend on configuration, i.e., on the state of long- and short-range order in the phase considered, the state of order being determined by minimizing the CVM free-energy functional with respect to cluster correlations.

Computation of a coherent phase diagram, that is, a phase diagram composed of phases that are based on one lattice only, requires knowledge of $F_{\rm mix}$ only, $F_{\rm in}$ being a linear function of the composition. Thus the free energy of mixing is computed with the CVM. The incoherent Al-Li phase diagram requires $F^{\rm fcc}_{\rm lin}$ and $F^{\rm bcc}_{\rm lin}$ as well, or rather, it requires the difference of these two linear terms, $\Delta F^{\rm fcc\text{-}bcc}_{\rm lin}=F^{\rm fcc}_{\rm lin}-F^{\rm bcc}_{\rm lin}$.

C. Cluster variation approach

Let site occupation be denoted by the pseudospin variable σ_p equal to $+1$ if site p is occupied by an Li, -1 if occupied by a Al atom. A configuration is specified if the set $\{\sigma\}$ of occupation variables is given for all N sites of the crystal lattice. The density function

$$\rho(\sigma)=Z^{-1}\exp\left[\frac{-E(\sigma)}{k_BT}\right] \tag{7}$$

allows suitable macroscopic averages to be taken. In Eq. (7), Z is the partition function, $E(\sigma)$ is the energy of configuration σ, and k_B is Boltzmann's constant. The expectation value of the energy is thus

$$\langle E\rangle=\sum_{\{\sigma\}}\rho(\sigma)E(\sigma)\ , \tag{8}$$

the sum being carried out over all configurations. The basic idea of the CVM is to express the density function $\rho(\sigma)$ as a linear function of cluster variables;[21] thus

$$\rho(\sigma)=\rho^0_N\sum_{\gamma,p}\Phi_{\gamma,p}(\sigma)\xi_{\gamma}\ , \tag{9}$$

where $\rho^0_N=2^{-N}$, and $\Phi_{\gamma,p}$ are the cluster products:

$$\Phi_{\gamma,p}(\sigma)=\sigma_{p+1}\sigma_{p+2}\cdots\sigma_{p+n}\ ,$$

where n_{γ} is the number of points in the cluster of type γ. The summation in Eq. (9) is extended to clusters of all types γ, including the "empty" cluster, located at all points p in the lattice. The cluster product of the "empty" cluster is equal to unity. The cluster correlations are given by

$$\xi_{\gamma}=\left\langle\rho^0_N\sum_{p}\Phi_{\gamma,p}(\sigma)\right\rangle\ , \tag{10}$$

where the average is defined as in Eq. (8). The multisite correlations ξ_{γ} are the independent variables of the problem, those with respect to which minimization of the CVM free-energy functional is performed. The set of multisite correlations is determined by the symmetry of the phase being considered.

When expression (9) for ρ is inserted in (8), an expression for the energy of a given ordered superstructure ψ_l is obtained (henceforth, brackets are not used in average values, for simplicity):

$$E^{\psi_l}=\sum_{\gamma}J_{\gamma}\xi^{\psi_l}_{\gamma}\ , \tag{11}$$

where the summation includes the "empty" cluster, designated by the index $\gamma=0$. The parameters J represent the effective cluster interactions which will be discussed in more detail below. The CVM free energy is obtained by adding to the energy E^{ψ_l} the term $-TS^{\psi_l}_{\rm conf}$, where the CVM configuration entropy is given by Refs. 21–23:

$$S^{\psi_l}_{\rm conf}=-k_B\sum_{\gamma}\Gamma^{\psi_l}_{\gamma}a_{\gamma}\sum_{\zeta}\rho_{\gamma}(\zeta)\ln\rho_{\gamma}(\zeta)\ , \tag{12}$$

where k_B is Boltzmann's constant, $\Gamma^{\psi_l}_{\gamma}$ is the number of clusters of type γ per lattice point in the ψ_i structure, a_{γ} are the Kikuchi-Barker coefficients[24] whose algebra is defined in Ref. 21; the summations are over all types of clusters γ and over all configurations (ζ) of the partial density matrices. The CVM approximation consists of limiting the sum to clusters contained within a (small) maximal cluster.

D. Connolly-Williams with volume dependence

The Connolly and Williams method[12] for obtaining effective cluster interactions from cohesive energies is intimately linked to the CVM. Combining (8) and (9) yields expressions for the effective cluster interactions for each lattice:

$$J_\gamma = \rho_N^0 \sum_{\sigma,p} \Phi_{\gamma,p}(\sigma) E(\sigma) \ .$$

This formula is exact, provided that the summation is extended over the infinite crystal. The CVM approximation, which consists of limiting cluster interactions to just a maximal cluster, provides a much more practical version of these formulas: The derivation starts with a cluster expansion, analogous to (11):

$$E^\psi_{\rm coh}(V) = \sum_{\gamma}^{\gamma_{\max}} \xi^\psi_\gamma J_\gamma(V) \ , \tag{13}$$

where $J_\gamma(V)$ and ξ^ψ_γ are the configuration-independent cluster interactions and the multisite correlation functions, respectively, associated with cluster γ, V is the molar volume of the alloy, and the sum runs, in principle, over all clusters in the crystal up to a maximum cluster which covers the entire macroscopic crystal. For brevity, the subscript of ψ will be considered implicit when dealing with superstructures. In practice, the expansion is assumed to be rapidly convergent, compatible with truncation of the sum at some small maximal cluster $\gamma_{\max}$ (CVM approximation). The system of linear equations (13) can be inverted to yield effective cluster interactions provided that the cohesive energies of a number of ordered structures are known, as mentioned above. Inversion is possible only if the number of cluster variables, that is, effective cluster interactions, is less than or equal to the number of cohesive energies. It is easy to show that the cluster variables required for a given approximation are those of the maximal cluster and all its subclusters. In the present case the cluster correlation for the fcc lattice are the tetrahedron, the triangle, the pair, the point, and the "empty" cluster. For the bcc lattice these are the tetrahedron, the triangle, the nearest-neighbor pair and next-nearest-neighbor pair, the point, and the "empty" cluster. Therefore, five J_γ parameters must be determined for the fcc case and six for the bcc. To obtain solutions of the linear system (13), it follows that at least five energy-versus-volume calculations must be performed for the fcc case, six for the bcc case, pertaining to the pure elements in both fcc and bcc structures and to stoichiometric ordered superstructures. By formally inverting (13) one arrives at the following explicit equation for the volume-dependent cluster interactions:

$$J_\gamma(V) = \sum_{\psi} (\xi^\psi_\gamma)^{-1} E^\psi_{\rm coh}(V) \ ,$$

or in matrix form,

$$\bar{J}(V) = \overline{\overline{\xi^{-1}}} \cdot \overline{E_{\rm coh}}(V) \ . \tag{14}$$

E. Volume-dependent cluster interactions

By expanding the cohesive energy as function of volume (V) around the equilibrium volume (V_0) and retaining only terms up to second order, one obtains

$$E^\psi_{\rm coh}(V) = E^\psi_{\rm coh}(V_0^\psi) + \frac{1}{2}\frac{B^\psi}{V_0^\psi}(V - V_0^\psi)^2 \ , \tag{15}$$

where $E_{\rm coh}(V_0)$ is the cohesive energy at the equilibrium volume (V_0) and where B represents the bulk modulus, the superscript ψ denoting the phase in question. Different phases are expanded about different equilibrium volumes. In order to allow a straightforward description in matrix notation, Eq. (15) is rewritten as an expansion around $V=0$:

$$E^\psi_{\rm coh}(V) = E^{(0)\psi} + E^{(1)\psi} + E^{(2)\psi} V^2 \ , \tag{16}$$

where

$$E^{(0)\psi} = E^\psi_{\rm coh}(V_0^\psi) + \tfrac{1}{2} B^\psi V_0^\psi \ ,$$

$$E^{(1)\psi} = -B^\psi \ ,$$

$$E^{(2)\psi} = \frac{1}{2}\frac{B^\psi}{V_0^\psi} \ .$$

This means that the vector $\overline{E_{\rm coh}}(V)$, with index ψ, can simply be rewritten as the product of a matrix E and a volume-dependent vector:

$$\overline{E_{\rm coh}}(V) = \begin{bmatrix} E^{(0)\psi_1} & E^{(1)\psi_1} & E^{(2)\psi_1} \\ E^{(0)\psi_2} & E^{(1)\psi_2} & E^{(2)\psi_2} \\ E^{(0)\psi_3} & E^{(1)\psi_3} & E^{(2)\psi_3} \\ \vdots & \vdots & \vdots \end{bmatrix} \begin{bmatrix} 1 \\ V \\ V^2 \end{bmatrix} \ . \tag{17}$$

Using expression (13), one obtains a simple parabolic volume dependence for the cluster interactions:

$$\bar{J}(V) = \begin{bmatrix} J^{(0)}_{\gamma_1} & J^{(1)}_{\gamma_1} & J^{(2)}_{\gamma_1} \\ J^{(0)}_{\gamma_2} & J^{(1)}_{\gamma_2} & J^{(2)}_{\gamma_2} \\ J^{(0)}_{\gamma_3} & J^{(1)}_{\gamma_3} & J^{(2)}_{\gamma_3} \\ \vdots & \vdots & \vdots \end{bmatrix} \begin{bmatrix} 1 \\ V \\ V^2 \end{bmatrix} \ , \tag{18}$$

where the interaction matrix $\overline{\overline{J}}$ is given by the product of the matrices $\overline{\overline{\xi^{-1}}}$ and E.

F. Introduction of volume-dependent interactions in the CVM

In the cluster variation method (CVM),[25] a free-energy expression is minimized with respect to a set of correlation functions. The minimization takes the form of finding the roots of the set of first derivatives of the free energy with respect to the correlation functions. Two techniques are used to solve the systems of nonlinear equations: the natural iteration method[26,27] and the Newton-Raphson method (NR).[23,28] The latter will be used in this work.

The set of correlation functions can be denoted by a vector ($\bar{\xi}$). The set of first derivatives of the Helmholtz free energy with respect to the correlation functions can be represented by a vector ($\bar{F'}$), and the set of second derivatives can be represented by a Hessian matrix ($\overline{\overline{F''}}$). In the NR method the minimum value of the free energy F and the corresponding vector ($\bar{\xi}$) are found by iteratively improving on an approximate solution ($\bar{\xi}_i$), according to

$$\overline{\xi_{i+1}} = \overline{\xi_i} - \overline{\overline{F''}}^{-1} \cdot \overline{F'} \ .$$

Starting with an initial guess $\overline{\xi_0}$, new approximations $\overline{\xi_{i+1}}$ are computed until the norm of the vector $\overline{F'}$ vanishes. The NR method exhibits rapid quadratic convergence and is especially advantageous because simple analytical expressions for $\overline{F'}$ and $\overline{\overline{F''}}$ are available.

The fact that in the present investigation the cluster interactions are volume dependent adds an extra degree of freedom. In this case the free-energy expression is not only to be minimized with respect to the correlation functions, but with respect to the volume as well. It will be shown that the Newton-Raphson technique is very well suited to include this additional minimization. Optimizing the Helmholtz free energy (F) with respect to volume can be performed conveniently with volume-dependent interactions of the form of (18). In the CVM expression for $F(=E-TS)$, only the energy (E) is an explicit function of the volume via the cluster interactions. The energy is of the following form:

$$E = \sum_{\gamma=0}^{\gamma_{\max}} \xi_\gamma J_\gamma(V) \ . \tag{19}$$

Because of the parabolic volume dependence of J_γ, one can easily compute the first- and second-order partial derivatives of the energy (or Helmholtz free energy for that matter) with respect to volume. By increasing the dimension of the cluster correlation function space by one, so as to include the volume, one can accomplish a joint-minimization of F with respect to both the correlation functions and volume. The Hessian of the Helmholtz free energy then has the form

$$\overline{\overline{F''}} = \begin{vmatrix} \dfrac{\partial^2 F}{\partial \xi_{\gamma_i} \partial \xi_{\gamma_j}} & \dfrac{\partial^2 F}{\partial V \partial \xi_{\gamma_j}} \\ \dfrac{\partial^2 F}{\partial \xi_{\gamma_i} \partial V} & \dfrac{\partial^2 F}{\partial V^2} \end{vmatrix} \ . \tag{20}$$

An alternative to a joint minimization is to perform the minimizations over the correlations and volume separately, as in the study by Terakura and co-workers.[10] The advantages of a joint minimization over two separate minimizations are twofold: (i) instabilities due to volume effects or due to the interplay of volume and correlation functions are easily determined by checking for negative eigenvalues of the Hessian. Instabilities which have corresponding eigenvectors that have at the same time both a nonzero volume component and nonzero cluster correlation function components can only be detected in a joint minimization; and (ii) the joint minimization is computationally much faster and leads to less complicated computer codes.

G. Relaxation

In the previous treatment the implicit assumption was made that element A will occupy the same molar volume in the alloy as element B. This statement becomes clear when a schematic outline of the computation is considered: Although cumbersome and impractical, the interactions J_γ could have been calculated at each possible volume V' by computing the energy of cohesion of the set of ordered compounds at that given volume V', followed by direct inversion to extract the interactions. The compression of both elements (and all ordered compounds in question) to the same molar volume V' means that the A and B atoms are forced to occupy the same volume as is illustrated in Fig. 2. Next, in the CVM, the A and B atoms are allowed to form different configurations, but no relaxation, i.e., redistribution of volume between A and B atoms, is allowed. In short, the model of alloying is the following: (1) An amount $(1-c)$ of element A is compressed or expanded to such an extent that its molar volume becomes equal to the volume of 1 mol of the alloy (V_{alloy}) to be prepared. A similar compression or expansion is performed on an amount c of element B (step 1 in Fig. 3). The amount of work required to change the molar volumes of element A and B from their respective equilibrium values V_A and V_B to the alloy volume usually is called the elastic energy (E^{elas}). (2) Next, the two pieces of compressed pure A and B are brought together, and while keeping the volume constant, the A and B atoms are mixed until an equilibrium state of (dis)order is attained (step 2 in Fig. 3). The energy involved in isochoric mixing is called the chemical energy (E^{chem}). It is clear that in this process the molar volumes of element A and B in an alloy will always end up here being the same. This restriction has not been considered in previous Connolly-Williams-type phase equilibrium studies.[10,12,13]

From various theories of alloying,[29] such as the Hume-Rothery rules, it is known that size effects, i.e., differences in molar volume, are significant with regard to phase stability. The problem of size effects or relaxation is a very complicated one, and here only a most simple

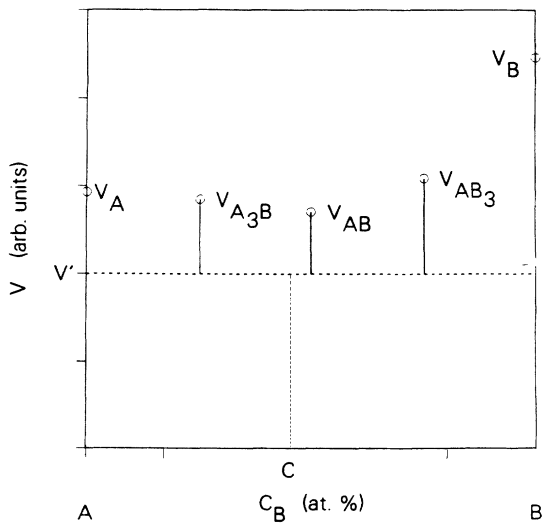

FIG. 2. Schematic representation of a step performed in computing cluster interactions. In order to calculate the cluster interactions for an alloy with concentration c and volume V', all ordered compounds are compressed from their equilibrium volumes V^0 to the volume of the alloy under consideration V'.

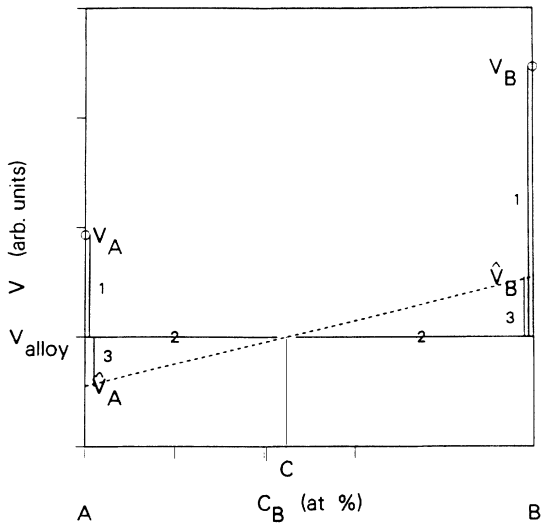

FIG. 3. Schematic outline of the model of alloying that includes relaxation effects. (1) The pure elements are compressed from their respective equilibrium molar volumes $V^0_{A,B}$ to the molar volume of the alloy V_{alloy}. (2) While keeping the total volume of the alloy constant (at V_{alloy}), the originally separated A and B atoms are mixed until a new equilibrium state of (dis)order is attained. (3) While keeping the volume of the alloy and the state of order constant, the molar volumes of element A and B ($\hat{V}_{A,B}$) are rearranged.

model is used to estimate its effect on phase equilibria.

To relax the assumption that both elements have the same molar volume in the alloy, an additional step in the previous mentioned model of alloying is suggested. After isochoric mixing has occurred, (3) the molar volumes of elements A and B are redistributed as is symbolically indicated by step 3 in Fig. 3. The molar volume of A in the alloy $\hat{V}_A$ is not necessarily equal (any more) to the molar volume of B in the alloy $\hat{V}_B$ or the molar volume of the alloy V_{alloy}. The two unknown variables $\hat{V}_A$ and $\hat{V}_B$ are determined by using two constraining assumptions: (a) the volume of the alloy remains constant during molar volume redistribution (relaxation); that is,

$$V_{\text{alloy}}=(1-c)\hat{V}_A+c\hat{V}_B \ , \tag{21}$$

and (b) the energy associated with this relaxation step E^{relax} can be approximated by the energy required to form a segregated alloy with an amount $(1-c)$ of element A and an amount c of element B at the volume of the alloy V_{alloy} from the pure elements, each at the volume of the alloy V_{alloy}. The relaxation energy is minimized with respect to the molar volumes $\hat{V}_A$ and $\hat{V}_B$:

$$E^{\text{relax}}=(1-c)\frac{B_A}{2V_A}[(V_A-\hat{V}_A)^2-(V_A-V_{\text{alloy}})^2] +c\frac{B_B}{2V_B}[(V_B-\hat{V}_B)^2-(V_B-V_{\text{alloy}})^2] \ . \tag{22}$$

The assumptions made are that (i) redistribution of molar volumes leaves the volume of the alloy unaffected, (ii) the redistribution does not affect the chemical order, and (iii) the energy involved in this relaxation step E^{relax} can be approximated by Eq. (22). Assumptions (1) and (2) are justified to some extent because the relaxation energy tends to be much smaller than the chemical and elastic energies, so that changes in alloy volume and chemical order are expected to be minor. Note that a theory recently proposed by Ferreira, Mbaye, and Zunger[13] is based on a much more stringent premise: The chemical order and the volume of the alloy, and therefore the elastic energy, are assumed to be independent of each other. The third assumption is not easy to justify. Equation (22) is rigorously correct if the atom in the alloy could be thought of as jellium soft spheres with elastic properties of the (bulk) pure elements.

Minimizing E^{relax} with respect to the relaxed molar volumes and using (21), the following equation is obtained:

$$E^{\text{relax}}=QW^2 \ , \tag{23}$$

where W is the difference of the alloy volume and the ideal volume: $W=V_{\text{alloy}}-(1-c)V_A-cV_B$, and where Q is a concentration-dependent elastic constant of the alloy given by

$$Q=-\frac{B_AB_B}{2[(1-c)B_BV_A+cB_AV_B]} \ . \tag{24}$$

An important aspect of relaxation is that the redistribution of molar volumes implies that the atomic volumes of A and B atoms are different, which results in a deformed lattice. In such a distorted lattice all lattice sites are no longer equivalent. True fcc and bcc Ising models, which the CVM solves in an approximate fashion, require equivalency of lattice sites. For that reason the configurational part of the free energy is dealt with by the CVM before relaxation is taken into account.

Introducing relaxation as previously described in the formalism of the CVM requires two steps: The first one is calculating the cluster interactions by applying the direct inversion scheme on the "unrelaxed" cohesive energies of a set of ordered phases. The unrelaxed cohesive energies are obtained by subtracting the relaxation energies from the cohesive energies as computed by total-energy methods. The volume dependence of the relaxation energy has some subtle effects. For example, the bulk modulus of an unrelaxed ordered compound is not the same as the bulk modulus computed for the relaxed compound. Because relaxation energies are second-order polynomial functions of volume, the cluster interactions J_γ still have the same algebraic form as put forward in Sec. II F. The second step is calculating the configurational free energy with the CVM and adding the relaxation (free) energy to obtain the cohesive free energy. Last, the cohesive free energy is minimized with respect to the cluster correlation functions and volume.

H. Vibrational entropy

Lithium has an allotropic transformation from bcc to a close-packed hexagonal (CPH) structure [9R (Ref. 30)] when the temperature drops below 78 K.[31] When bcc

lithium is deformed while cooling, however, an fcc phase is formed at temperatures below about 110 K.[32] It appears that although the 9R CPH structure is the stable one at low temperatures, the energy difference with the fcc structure is very small. For that reason we will assume that the CPH structure can be represented by the fcc structure. This can be justified also on the grounds that the interatomic distances in 9R CPH lithium and fcc lithium are the same and that 9R CPH and fcc structures differ only in the stacking of the $\{111\}$ planes. The fact that lithium has an allotropic transformation at 78 K from CPH to bcc indicates that differences in vibrational entropy cannot be neglected. Table I shows fcc lithium as the more stable form at 0 K, although the difference with the bcc modification is only slight, as required. Unless a vibrational entropy difference for the fcc and bcc forms is invoked, the fcc structure will remain the stable structure for lithium at all temperatures in the phase diagram computation. The theories concerning vibrational entropy require a detailed knowledge of elastic constants,[33,34] which are not available for unstable structures and lead to very extensive computations in the context of an intricate theory like the CVM.[34] In the absence of applicable theories concerning vibrational entropy, we assume a simple empirical form, namely, that the difference in the vibrational entropy between fcc and bcc lattices is a linear function of alloy composition and is independent of temperature. The vibrational entropy difference $\Delta S_{\rm vib}=S_{\rm vib}^{\rm bcc}-S_{\rm vib}^{\rm fcc}$ for elemental lithium can then be computed from the cohesive energy difference of fcc and bcc allotropes at 0 K and from the experimental observation that the transition occurs at 78 K.[31] This yields a $\Delta S_{\rm vib}^{\rm Li}$ of $1.01R$, where R is the universal gas constant.

For aluminum the situation is more difficult since no bcc modification has been observed at ordinary pressures. Therefore, we resort to the fictitious fcc-bcc transition at 2080 K as predicted from (sub)regular solution model type phase diagram computations by Kaufman and Bernstein.[35] This results in a $\Delta S_{\rm vib}^{\rm AL}$ of $0.346R$. Assuming a linear concentration dependence of $\Delta S_{\rm vib}$, one obtains

$$\frac{\Delta S_{\rm vib}(c)}{R}=0.346+0.664c\ , \tag{25}$$

where c denotes the atomic concentration of lithium. Note that our empirical estimate for the vibrational entropy difference is in excellent agreement with a theoretical calculation by Friedel,[36] which results in a value of $0.6R$.

TABLE I. FLAPW results for fcc- and bcc-based structures. The cohesive energy $E_{\rm coh}$ is defined as the difference of the energy of 1 mol of atoms in the solid state and the energy of 1 mol of atoms in the infinitely diluted gas state (infinite interatomic distances). The equilibrium molar volume and bulk modulus are represented by V and B, respectively.

Structure	$E_{\rm coh}$ (kJ/mol)	V_0 (cm^3/mol)	B (GPa)
Al (fcc)	387.164	9.5533	82.198
Al_3Li ($L1_2$)	342.297	9.4518	70.305
AlLi ($L1_0$)	288.765	9.2805	50.409
$AlLi_3$ ($L1_2$)	225.911	9.7403	28.370
Li (fcc)	164.108	11.4031	13.642
Al (bcc)	381.125	9.6068	84.184
Al_3Li ($D0_3$)	329.299	9.6518	55.844
AlLi ($B2$)	289.027	8.8921	42.091
AlLi ($B32$)	297.167	9.2148	57.750
$AlLi_3$ ($D0_3$)	230.244	9.6829	29.640
Li (bcc)	163.452	11.4387	15.246

I. Liquid free energy

Although techniques such as the density functional theory[37] have made significant progress in the modeling of liquids, application in a first-principles method does not yet appear possible. Therefore, a regular solution formula[35] for the free energy of the liquid phase is assumed here:

$$F_{\rm liq}(c,T)=cF_{\rm liq}^{\rm Li}(T)+(1-c)F_{\rm liq}^{\rm Al}(T)+Lc(1-c)+Rt[c\ln c+(1-c)\ln(1-c)]\ , \tag{26}$$

where L is a fitting parameter, in this case used to fit the melting point of $B32$ AlLi at its experimental value[38] of 990 K and where $F_{\rm liq}^{\rm Al,Li}$ are given by

$$F_{\rm liq}^{I}(T)=E_I^{\psi}+\Delta E_I^{\psi\rightarrow\rm liq}-T\frac{\Delta E_I^{\psi\rightarrow\rm liq}}{T_I^{\psi}}\ , \tag{27}$$

where the index I refers to either Al or Li, the superscript ψ denotes the bcc structure for Li and the fcc structure for Al, and E_I^{ψ} refers to the cohesive energy of element I with structure ψ at 0 K. T_I^{ψ} is the experimentally observed melting temperature, and $\Delta E_I^{\psi\rightarrow\rm liq}$ represents the latent heat of melting.[39] The latent heat divided by the melting temperature is used as an estimate for the entropy of melting. The values of the melting points and latent heats are listed in Table II. It follows that three melting points are fitted: the melting points of the pure elements plus the melting point of stoichiometric $B32$ AlLi.

III. RESULTS AND DISCUSSION

A. FLAPW results

Table I and Fig. 4 show results from the total-energy FLAPW calculation. As mentioned above, first-

TABLE II. Properties of melting for bcc lithium and fcc aluminum. $E_{\rm melt}$ and $T_{\rm melt}$ are the experimentally observed latent heat of melting and the melting temperature, respectively (Ref. 39). The entropy of melting $S_{\rm melt}$ is calculated as the ratio of the latent heat over the melting temperature.

Phase	$\Delta E_{\rm melt}$ (kJ/mol)	$T_{\rm melt}$ (K)	$\Delta S_{\rm melt}$ (J/mol K)
Al-fcc	10.753	933.35	11.521
Li-bcc	2.887	452.15	6.385

principles cohesive energies, equilibrium volumes, and bulk moduli are obtained for a number of fcc and bcc superstructures. Note that the calculated properties all pertain to a temperature of 0 K. The practical usefulness of first-principles calculations is very evident here, for not only do these computations greatly increase our understanding of the solid state, but accurately computed first-principles results also provide an alternative where experimental data is insufficient or completely lacking. Many of the properties listed in Table I are only very approximately or not at all known from experiment. Cohesive energies, for example, can be compared to experimental data in only two cases. We will compare the calculated cohesive energies with sublimation energies at 0 K. Reference 40 gives the values 321.9 and 161.6 kJ/mol for the sublimation energies of fcc aluminum and bcc lithium at 298 K. The sublimation energy at 0 K ($E^0_{\rm sbl}$) can be obtained from the sublimation energy at 298 K ($E^{298}_{\rm sbl}$) with the following expression:

$$E^0_{\rm sbl}=E^{298}_{\rm sbl}+\int_0^{298} c_p^{\rm solid}\,dT-\int_0^{298} c_p^{\rm vapor}\,dT\ .$$

Unfortunately, no accurate values for the isobaric specific heat c_p for the pure elements between 0 and 298 K are available. Therefore, the specific heat of the pure elements for temperatures above 298 K has been extrapolated to the temperature range 0–298 K. The temperature dependence of c_p for the pure elements is given by the following expressions:[40]

$$c_p(\mathrm{Al})=4.186(4.94+0.002\,96T)\ ,$$
$$c_p(\mathrm{Li})=4.186(3.33+0.008\,21T)\ .$$

The units are K for temperature and J/mol K for the specific heat. The c_p of the vapor phase is approximated by the value for the ideal monoatomic gas[41] of $\frac{5}{2}R$. Using these expressions for c_p, values for the sublimation energy $E_{\rm sbl}$ at 0 K are obtained. The sublimation energy for Al-fcc is 322.4 kJ/mol, to be compared with a cohesive energy of 387.2 kJ/mol. The corresponding numbers for Li-bcc are 161.1 and 164.1 kJ/mol. These values for both Al-fcc and Li-bcc are seen to compare reasonably well with 17% and 2% difference, respectively. Note that the temperature correction for the sublimation energy is of little significance.

The energy difference between the fcc and bcc structures, defined as $\Delta E^{\rm fcc-bcc}=E^{\rm fcc}_{\rm coh}-E^{\rm bcc}_{\rm coh}$, is given in Table III. The $\Delta E^{\rm fcc-bcc}$ value for Li (0.656 kJ/mol) is small and positive, in accordance with the fact that in actuality the bcc form of Li is not the ground state, and that the bcc becomes only stable at elevated temperatures by merit of its large vibrational entropy. The smallness of $\Delta E^{\rm fcc-bcc}$ is to be expected; upon cooling (below 110 K) the fcc allotrope forms when the bcc modification is deformed. The structural energy difference predicted with phase diagram fitting,[1,35] −1.214 kJ/mol, does not describe the behavior of Li: The negative sign would indicate that the bcc form is always more stable than the fcc

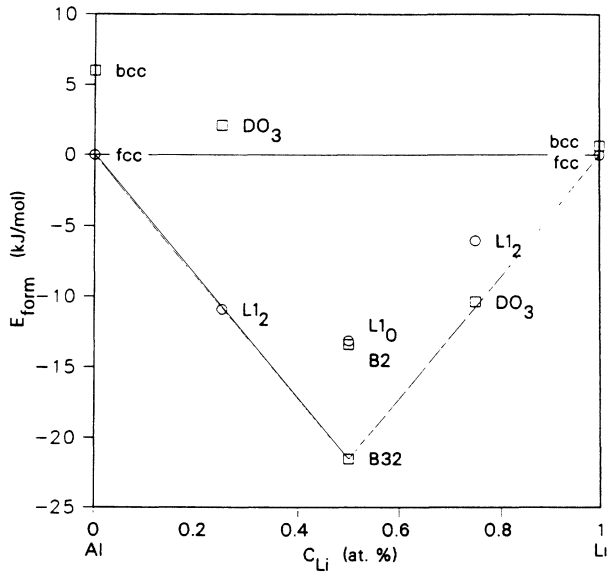

FIG. 4. Formation energy $E_{\rm form}$ as a function of composition. This plot shows the phase equilibria at 0 K. The circles and squares correspond to structures based on the fcc and bcc lattices, respectively. The Al_3Li-$L1_2$ phase is just below the (solid) line connecting the Al-fcc and $B32$ phases, an indication that the $L1_2$ phase is just stable at 0 K. The $AlLi_3$-$L1_2$ phase is far above the (dashed) line connecting the Li-fcc and $B32$ phases, indicating that this $L1_2$ phase is not stable at 0 K (nor at any other temperature).

TABLE III. Comparison of various physical properties computed with the FLAPW method (this work) with available experimental data (sources listed in references). Units are kJ/mol for the structural energy difference $\Delta E^{\rm fcc-bcc}$ and for the energies of sublimation, cohesion, and formation, $E_{\rm sbl}$, $E_{\rm coh}$, and $E_{\rm form}$, respectively, and cm^3/mol and GPa for the equilibrium volume V_0 and the bulk modulus B. The bulk moduli are followed by the temperature in brackets. For the structural energies and formation energy, no experimental data were available; instead a comparison is made with results obtained from phase diagram fitting (listed under "fitting").

Property	Phase	FLAPW	Experiment	Reference
$E_{\rm coh}$::$E_{\rm sblm}$	Al-fcc	387.2	322.4	40
	Li-bcc	164.1	161.1	40
V_0 (298 K)	Al-fcc	9.5533	9.7861	40
	$B32$	9.2148	9.3849	40
	Li-bcc	11.4387	12.391	40
	Li-fcc	11.4031	12.288	40
	Al_3Li-$L1_2$	9.4518	9.439	15
B	Al-fcc	82.2 (0 K)	83.3 (0 K)	38
			75.2 (295 K)	38
			76.6 (295 K)	44
			77.3 (295 K)	40
	Al_3Li-$L1_2$	70.3 (0 K)	66.0 (295 K)	44
	Li-bcc	15.2 (0 K)	12.0 (295 K)	40

Property	phase	FLAPW	fitting	
$\Delta E^{\rm fcc-bcc}$	Al-bcc	6.039	10.086	1,35
	Li-bcc	0.656	−1.214	1,35
$E_{\rm form}$	$B32$	−21.531	−15.633	4
			−23.685	1

form, in contradiction with the fcc-bcc transformation of Li at low temperatures, just mentioned.

The large positive value of the structural energy difference predicted by the FLAPW calculations for Al (6.039 kJ/mol) indicates that the fcc modification is the more stable form at all temperatures (below the melting point). The value predicted by phase diagram fitting[1,35] is again significantly different (10.086 kJ/mol). However, a recent study of Miodownik[42] has shown that phase diagram fitting is not always able to predict structural energy differences accurately.

The calculated formation energies, defined in (3) (Table III), of the competing phases at equiatomic composition strongly favor the $B32$ phase, as is observed in actual Al-Li alloys. The computed value for E_{form} of -21.531 kJ/mol for the $B32$ phase compares well with phase diagram fitting results: -15.633 kJ/mol (Ref. 4) and -23.685 kJ/mol.[1] Note that the two phase diagram fitting results differ significantly from each other. Our faith in the first-principles formation energies is further strengthened by the fact that the Al_3Li-$L1_2$ phase is predicted to be only just stable with regard to a mixture of the Al-fcc and AlLi-$B32$ phases. Figure 4 shows that at 0 K the Al_3Li-$L1_2$ phase is virtually on (but just below) the line connecting the formation energies of Al-fcc and AlLi-$B32$. This means that the $L1_2$ is likely to become a metastable phase at temperatures only just above 0 K, in agreement with experimental observations in Al-rich alloys. This is an important point because the formation of $L1_2$ precipitates is of great significance for the technological application of Al-Li alloys. The stability of the $L1_2$ phase will be discussed in more detail below.

The first-principles values of the equilibrium molar volumes V_0 differ by less than 10% from those obtained from lattice-parameter measurements[16,40] (see Table III). Note that the error in the molar volume is 3 times larger than the error in the lattice parameter. Since lattice parameters are measured at 298 K and total-energy computations yield values for the molar volume at 0 K, the effect of thermal expansion must be taken into account. In the absence of experimentally determined linear thermal expansion coefficients for the intermediate phases in the Al-Li system, it has been assumed that the thermal expansion of an intermediate phase is given by the concentration (in at. %) weighted average of the thermal expansions of the pure elements. The linear thermal expansion coefficients of Al-fcc and of Li-bcc are 23.5×10^{-6} and 56.0×10^{-6} K^{-1}, respectively.[40] Correcting in this fashion for thermal expansion yields the following experimental molar volumes: For Al-fcc the experimental V_0 is 9.7861 cm^3/mol, from which the calculated value deviates by less than 2.5%. For the $B32$, Li-bcc, and Li-fcc phases, the experimental values are 9.3849, 12.391, and 12.288 cm^3/mol, which differ by 2%, 9%, and 8% from the computed values. The molar volume for Al_3Li-$L1_2$ precipitates in a 4.5 at. % Li alloy has been determined[16] at 9.439 cm^3/mol, from which the computed value differs by only 0.14%. With the exception of the last phase, the FLAPW consistently (but slightly) underestimates the equilibrium molar volume. A recent study[43] has shown that this underestimation of lattice parameters by total-energy methods can be significantly diminished by taking the zero-temperature vibration of the ions into account.

Only in a few cases can first-principles and measured bulk moduli be compared due to the scarcity of experimental data. Mondolfo[38] reports the observed bulk modulus of pure fcc aluminum at two temperatures: 83.3 GPa at 0 K and 75.2 GPa at 295 K. More recently, Mueller, Bubeck, and Gerold[44] measured a bulk modulus of 76.6 GPa for fcc aluminum at room temperature. Another experimental value for the bulk modulus for Al-fcc can be obtained from the elastic constants given in the literature.[40] Under hydrostatic stress the bulk modulus equals $\frac{1}{3}(C_{11}+2C_{12})$, which results in a value of 77.3 GPa for Al-fcc at room temperature. Taking into account that the experimental room-temperature values of the bulk modulus should be multiplied by a factor of 1.04 to obtain the 0-K value,[45] an average experimental bulk modulus of 80.4 GPa is found. The first-principles bulk modulus of 82.2 GPa is in very close agreement with this value.

The bulk modulus of the Al_3Li-$L1_2$ phase cannot be measured directly because that phase exists only in the form of precipitates. Mueller, Bubeck, and Gerold[44] inferred from their measurements a bulk modulus of 66 GPa at room temperature. The first-principles value of 70.3 GPa at 0 K is in good agreement with experiment.

The bulk modulus of lithium can be calculated from (experimental) elastic constants[40] using the expression mentioned above. At room temperature a modulus of 12.0 GPa is obtained which compares favorably to the first-principles result of 15.2 GPa, which applies to a temperature of 0 K. Considering that Li is an element with a low melting point, and that therefore considerable softening will occur upon raising the temperature to 298 K, the first-principles value is in excellent agreement.

B. Phase diagrams

In this section Al-Li phase diagrams, the main results of this study, will be presented and discussed. The assessed Al-Li phase diagram, based on experimental data,[4] is shown in Fig. 1. Its main features include a very stable equiatomic $B32$ phase, an fcc Al-rich solid solution which has a significant solubility for lithium, a bcc Li-rich solid solution which contains almost no dissolved Al, and a metastable Al_3Li-$L1_2$ phase. Determination of the precise location of the phase boundaries concerning the $L1_2$ phase has proved to be an elusive problem due to experimental difficulties. We will show that the first-principles approach can be an extremely useful tool for a qualitative and quantitative description of both stable and metastable phase equilibria. Through a succession of first-principles phase diagrams, in which more and more phases and effects are taken into account, it will be shown that all the main features of the experimental phase diagram can be understood and even predicted.

An fcc Al-Li phase diagram can be obtained by comparing only the free energies of fcc and fcc-based superstructures (like $L1_0$ and $L1_2$). Figure 5 shows the first-principles fcc Al-Li diagram in which no relaxation has been taken into account. The dashed line indicates the

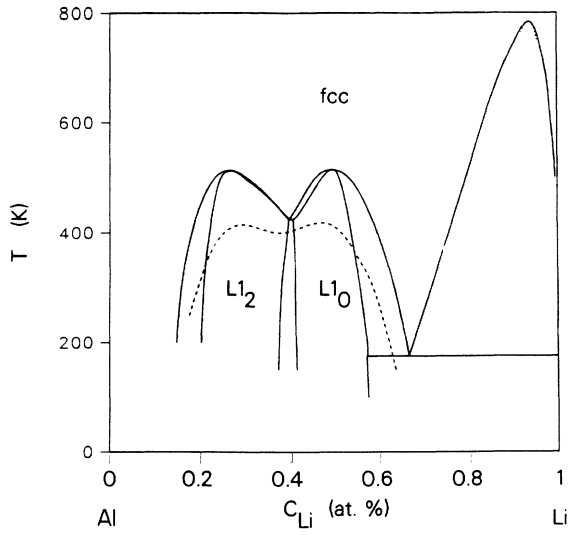

FIG. 5. Al-Li phase diagram calculated with only fcc-based structures taken into account. Relaxation effects, as described in Sec. II G, have not been included. The dotted line represents the [000] phase separation spinodal, and the dashed curve indicates the [100] ordering spinodal (Refs. 27 and 46).

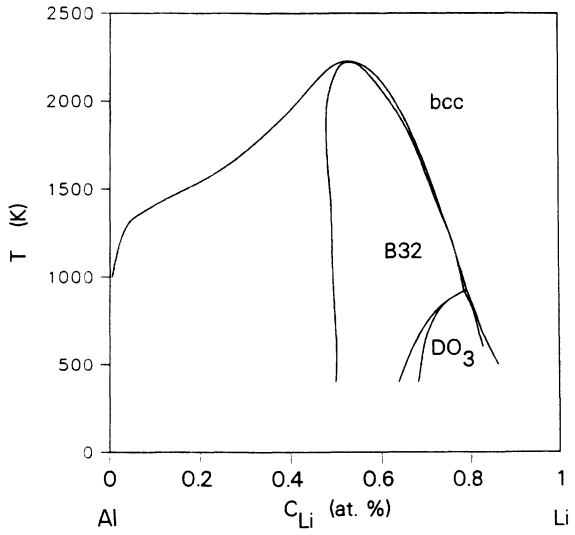

FIG. 6. bcc Al-Li phase diagram without relaxation. The dotted line indicates the metastable miscibility gap in the disordered bcc solid solution.

[100] ordering spinodal,[27,46] the meaning of which is as follows: If an alloy is cooled rapidly from the (metastable) fcc disordered state to a temperature situated below this spinodal, $\langle 100 \rangle$ ordering waves are expected to grow spontaneously in amplitude producing a microstructure more reminiscent of continuous ordering than of discrete nucleation and growth. High-resolution transmission electron micrographs obtained on Al-rich Al-Li alloys by Radmilovic and Thomas[47] appear to confirm that spinodal ordering is a viable transformation mechanism in this system. The main features of the diagram are a miscibility gap (MG) with a maximum temperature of 775 K and two ordered phases $L1_2$ and $L1_0$ with transition temperature of 520 and 515 K, respectively. The MG is caused by an elastic instability. This is evident from the fact that the eigenvector corresponding to the negative eigenvalue of the Hessian matrix has nonzero components only with respect to volume (all cluster correlation function components of these eigenvectors are zero). Another way to come to this same conclusion is to compute the phase diagram ignoring volume effects altogether. In that case a diagram is obtained that strongly resembles Fig. 5 except for one feature, the miscibility gap on the Li-rich side.

When relaxation (according to Sec. II G) is taken into account, only minute changes in the fcc phase diagram occur, the most significant of which is a lowering of the maximum temperature of the MG by some 25 K. The tendency toward phase separation is diminished because relaxation reduces elastic energies which caused the MG.

Figure 6 shows the phase equilibria between bcc and bcc-based superstructures (like DO_3 and $B32$), without relaxation. The diagram exhibits a very stable $B32$ phase with a transition temperature of 2230 K, a much less pronounced $AlLi_3$-DO_3 phase and a metastable MG for Al-rich alloys. When the bcc phase diagram is computed with relaxation taken into account, only insignificant differences with Fig. 6 are found. The origin of the negligible influence of relaxation in both the fcc and bcc Al-Li system is twofold: The bulk moduli of both elements are small, leading to small relaxation energies. Calculations show that relaxation energies in the Al-Li system are typically less than 2% of the total energy of alloying. (ii) The alloy molar volumes of ordered and disordered phases at the same composition differ only very slightly, resulting in only small differences in the relaxation energies for ordered and disordered phases. The competition between ordered and disordered phases is therefore virtually unaffected by relaxation effects. In other alloys, with larger bulk moduli, like Cu-Au, relaxation might have a much more pronounced effect. Because of its negligible contribution, relaxation has been neglected in all phase diagrams which are discussed in the remainder of this paper.

By combining the free energies of fcc- and bcc-based phases, a first-principles fcc-bcc Al-Li phase diagram was computed (see Fig. 7). This phase diagram is to be regarded as the main result of this study. Elemental Li remains fcc at all temperatures because no vibrational entropy has been included. Note, however, that the Li-rich side of the diagram is dominated by bcc-based $B32$ and DO_3 structures. Especially, the $B32$ phase is remarkably stable. It will be shown below that including a liquid phase causes the $B32$ phase to melt before disordering takes place. The DO_3 phase occurs quite far away from its stoichiometric composition due to the stronger ordering tendencies closer to equiatomic concentrations and the competition with fcc-Li. The bcc-based superstructures are much more stable than the fcc-based superstructures; Al_3Li-$L1_2$ is the only fcc ordered phase that is almost stable. The metastable fcc phase equilibria are shown in dashed lines.

This calculated phase diagram exhibits a striking

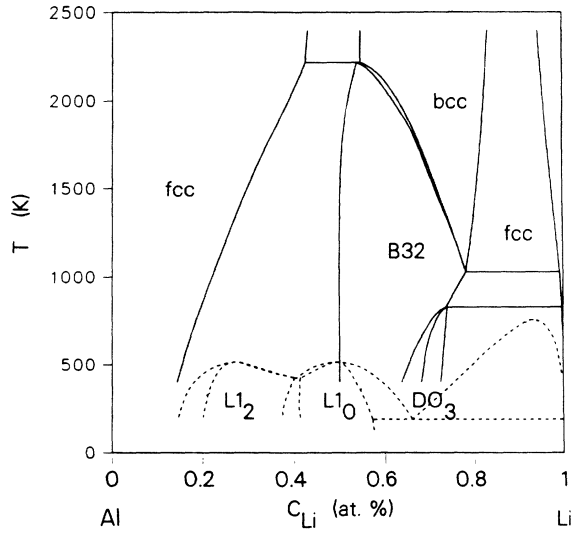

FIG. 7. Solid-state part of the Al-Li phase diagram. Both fcc- and bcc-based phases have been included. The fcc-based ordered phases have been repressed because of the greater stability of the bcc-based superstructures. The metastable fcc-based equilibria are indicated with dashed lines. The [100] fcc ordering spinodal is denoted with a dotted line. Note that at this stage no experimental data have centered the computation.

resemblance with the solid-state part of the experimentally observed diagram. A detailed comparison of the computed and actually observed phase diagrams will make clear that all the main features of the Al-Li system are correctly described. The fcc solid solution at the Al-rich side of the diagram is correctly predicted, and moreover, the solid solution also exhibits a marked solubility for Li which decreases when the temperature is lowered.[4]

The metastable Al_3Li-$L1_2$ phase, which can precipitate from oversaturated solid solutions, is correctly calculated to be metastable.[4] This is not in contradiction with the fact that, at 0 K, the formation energy of the $L1_2$ phase was located just below the line connecting the $B32$ and Al-fcc points in Fig. 4. At slightly higher temperature, the free energies of the two ordered phases can be considered to remain constant because the degree of order remains virtually perfect; the free energy of the Al-fcc solid solution, on the other hand, will decrease rapidly due to the increasing solubility of lithium and the corresponding increase in configurational entropy. This causes the line connecting the free energies of the $B32$ and Al-fcc solid solution (common tangent) to drop with increasing temperature, so that the free energy of the $L1_2$ phase ends up above the line (common tangent).

The order-disorder temperature of the $L1_2$ is predicted to be 520 K, which at the very least can be said to be of the right order of magnitude. Differential thermal analysis has indicated an effect at 800 K, which has been interpreted[48] as an $L1_2$ order-disorder transition. This interpretation appears questionable, as the highest temperature at which $L1_2$ has been directly observed[49] is 616 K. Computations show that the metastable two-phase region between the fcc solid solution and the $L1_2$ phase is narrower than is observed in actual alloys,[3] but the phase boundary at the $L1_2$ side of the two-phase region appears to be accurately reproduced at about 20 at. % Li.

The metastable miscibility gap (MG) at the Al-rich side of the phase diagram conjectured by Sigli and Sanchez[5] was not found in the present work. Unfortunately, comparison with experimental observation is not possible. A metastable clustering spinodal is unlikely to be observed when there is the slightest tendency toward ordering, as in the Al-Li system, because clustering requires diffusion over macroscopic distances, whereas ordering can occur by means of diffusion on an atomic scale.[27,46] Accordingly, there is no sound experimental evidence for a clustering spinodal. Recent *in situ* atomic resolution electron microscopy studies[47] have revealed, however, that ordering occurs before and during the initial stages of precipitation, in agreement with our results.

Our computations show that the center of the phase diagram is dominated by a very stable $B32$ phase, in complete agreement with observations in actual Al-Li alloys.[3,4]

This study, as outlined in Sec. II, does not include a description of the complex interloper phases Al_2Li_3 and Al_4Li_9. However, a phase with $D0_3$ structure can be described in our present model and appears to have characteristics which resemble the complex phase. The $AlLi_3$-$D0_3$ phase is calculated to be stable only over a narrow range of composition, just as in the two complex phases which appear in the experimental phase diagram as line compounds.[4] Furthermore, computations show that the $AlLi_3$-$D0_3$ phase does not occur at stoichiometry, but rather at compositions around $c_{Li} \approx 0.70$, where the Al_4Li_9 phase is observed.[4]

The solid solubility of Al in Li is computed to be virtually nil (of the order of 10^{-4}), in good agreement with other studies[3-5] which are based on experimental data. Li remains fcc right up to the melting point because vibrational entropy has not been included (in Fig. 9 we will include vibrational entropy). The fcc Li melting point is above the observed fcc Li melting point because, in the absence of vibrational entropy, the fcc structure remains more stable than the bcc structure at all temperatures. First-principles computation of the solid-state part of the Al-Li phase diagram has been remarkably successful; all the main features of the experimental phase diagram have, at least qualitatively, been reproduced. The quantitative agreement is not as good. Two relatively minor differences are that (i) the computed two-phase region between Al-rich solid solution and $L1_2$ is narrow, barely 5 at. % at ambient temperatures, whereas the observed two-phase region has a width of some 20 at. %;[4] (ii) our calculations show a slower decrease of the solid solubility of Li in Al than is observed experimentally,[3,4] so that at low temperature the solid solubility of Li in Al is significantly overestimated. The predicted solid solubility at higher temperatures is slightly too large also, but in better agreement with experimental observations.

More features of the experimental phase diagram can be reproduced when an empirical liquid free energy is included (see Sec. II I). The resulting computed phase diagram is shown in Fig. 8. The $B32$ phase is found to melt

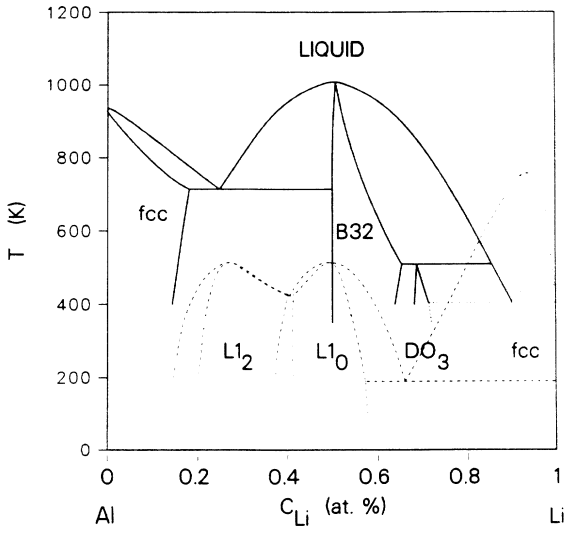

FIG. 8. Al-Li phase diagram in which a liquid phase, modeled with a regular solid solution model free energy, has been included. The vibrational entropy difference of the bcc- and fcc-based phases was not considered in this computation. The metastable fcc phase equilibria are indicated with dashed lines (superposition of Fig. 5). The [000] and [100] fcc spinodal curves are shown as dotted lines.

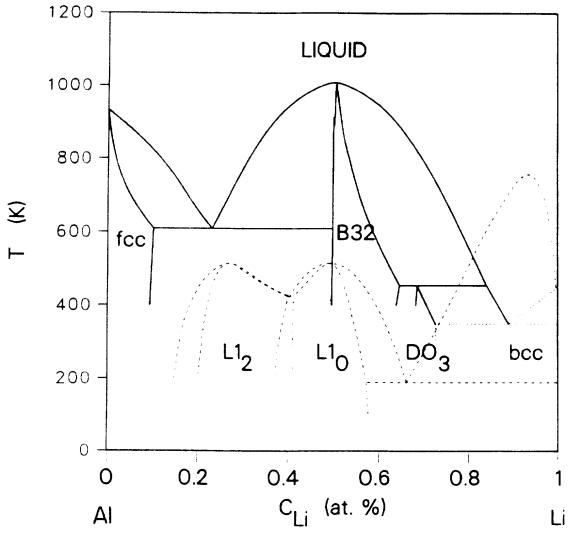

FIG. 9. As in Fig. 8, but now including the empirical vibrational entropy difference between fcc- and bcc-based phases.

congruently before undergoing a disordering reaction as is observed experimentally.[3,4] the computed phase diagram exhibits two eutectics, one at the Al-rich side and another at the Li-rich side, just like the experimental phase diagram. The calculated eutectic temperatures are much lower than the experimental values, some 150 K at the Al-rich side and about 50 K at the Li-rich side. The peritectic at about 70 at. % Li is another feature that is correctly predicted although the peritectic temperature is some 90 K lower than experiment indicates.

The consistent underestimation of eutectic and peritectic temperatures is caused by the particular form of the free-energy expression used for the liquid. As described in Sec. II I, the liquid free energy, given by a regular solution expression, contains an adjustable enthalpy term, which is used to fit the melting point of the $B32$ phase. The remarkable stability of the $B32$ phase requires a very negative enthalpy. This enthalpy is not a function of temperature, so that at temperatures below the $B32$ melting point the liquid free energy remains very low. Thus the liquid is stabilized at the expense of the solid, so that too low eutectic temperatures are computed. If, on the other hand, the $B32$ melting point were fitted with an excess entropy term, the liquid free energy would become less negative as the temperature decreased. The liquid would not be stabilized unjustly with respect to the solid phases, and higher eutectic temperatures would be found. In that case the Al-AlLi eutectic is computed at 845 K, just 25 K below the experimental eutectic temperature. Because both of these liquid free-energy expressions are fits and in no way related to first principles, we will not delve into this any further.

Figure 9 shows an Al-Li phase diagram in which vibrational entropy, as described in Sec. II H, has been included. Vibrational entropy significantly influences the phase diagram at higher temperatures, as can be seen by comparing Figs. 8 and 9. The solid solubility of Li in fcc Al has been decreased as compared with Fig. 8, so that now a better agreement with the experimental values (Fig. 4) is found. The occurrence of bcc Li above 78 K is now correctly described, as is the melting temperature. The stability of the $D0_3$ phase is somewhat reduced by vibrational entropy. Because the $D0_3$ phase does not occur in Al-Li alloys, this is neither an improvement nor a detriment.

Including the empirical vibrational entropy also slightly deteriorates some features of the diagram, namely, that the eutectic temperatures on both the Al- and Li-rich sides have further departed from their experimental values. The eutectics can be made more "agreeable" by using another fitting quantity in the regular-solution-type free-energy formula for the liquid as discussed above.

C. Prediction of lattice parameters and the enhanced modulus effect

Minimizing the Gibbs free energy with respect to alloy molar volume in the CVM allows the determination of the equilibrium volume (or lattice parameter) of alloys as a function of composition. The equilibrium volume also varies slightly with the state of order, although this effect is much less pronounced. The computations predict, for example, that the Al_3Li-$L1_2$ order-disorder transformation is accompanied by a volume change of about 0.14%.

Figure 10 illustrates how remarkably accurately this first-principles method can predict changes of lattice parameter with composition. The temperature of the experimental measurements is extrapolated to 0 K by the same method as used in Sec. III A. The predicted influence of Li on the lattice parameter of the $B32$ phase agrees well with experimental determinations[50,51] except for a constant factor. The difference between the experimental

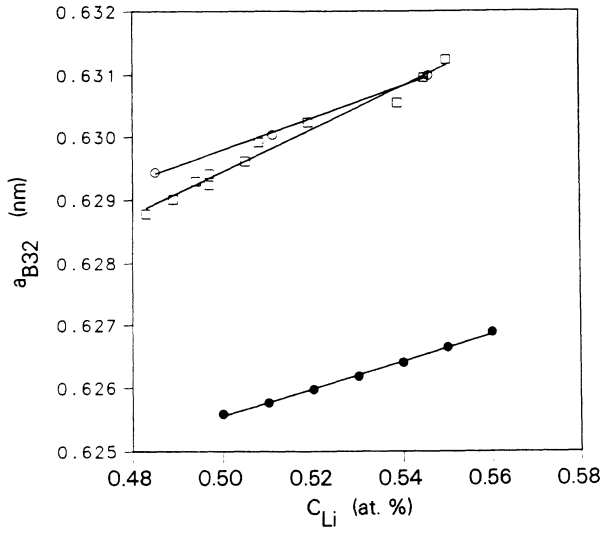

FIG. 10. Lattice parameter of the $B32$ phase a_{B32} as a function of the lithium concentration c_{Li} at 0 K. The solid points represent the theoretically predicted lattice parameters (Sec. II C), the open circles and squares indicate experimental measurements from Refs. 50 and 51 as quoted by Ref. 4. The experimental data have been extrapolated from 298 to 0 K as described in the text.

lattice-parameter measurements and the calculated results can be explained by the fact that the total energy computations typically predict the molar volumes of stoichiometric compounds with an accuracy of the order of a few percent. The predicted and experimentally determined lattice-parameter variations $\partial a_{B32}/\partial c_{\mathrm{Li}}$, in both cases computed by linear regression, are given in Table IV. The influence of the lithium content is surprisingly well predicted, especially when the variation between the two experimentally determined slopes is considered.[50,51]

Computations of the influence of Li on the lattice parameter of Al-rich solid solutions show that the lattice parameter decreases 51×10^{-6} nm per at. % Li in solid solution. This linear decrease of the lattice parameter has been observed in actual Al-Li alloys, although the reported rates of decrease vary considerably. A least-squares analysis of the data in Refs. 50, 52, and 53 yields rates of 29×10^{-6}, 44×10^{-6}, and 69×10^{-6} nm per at. % Li, respectively. It is clear that the experimental determinations differ as much among each other as they differ from the first-principles result. Comparison of these values may give the impression that none of these numbers are very accurate; however, when the deviations from Vegard's law are compared, the relative errors are found to be very small. Including relaxation in the calculations does not improve the correspondence between experiment and computation.

The misfit parameter, defined as the ratio of the lattice parameter of the precipitate ($L1_2$ phase) over the lattice parameter of the matrix (Al-rich solid solution) minus unity times 100%,

$$\delta=\left[\frac{a_{\mathrm{prec}}}{a_{\mathrm{matr}}}-1\right]\times100\% , \tag{28}$$

can be computed when the compositions of the coexisting phases are known. The compositions of Al-rich solid solutions (matrix) in equilibrium with Al_3Li-$L1_2$ (precipitate) have been taken from the experimental phase diagram (Fig. 4). At 300 K the matrix and precipitate contain 5 and 24 at. % Li, respectively; at 500 K the compositions are 8 and 21 at. % Li. At these compositions the lattice parameters have been computed so that the misfit parameter could be evaluated; results are listed in Table IV. Our computations predict that the misfit parameter is small and negative (see Table IV), the absolute value of which decreases with temperature. All three of these findings are in agreement with experiment.[49,54] Although the quantitative agreement between theoretical and experimental results may appear poor because there seems to be a large relative error, note that the difference (absolute error) is extremely small.

Many experiments[44,55–57] have conclusively shown that the Young's modulus of Al-rich solid solutions in-

TABLE IV. Comparison of theoretical CVM predictions and experimental measurements. The change of the lattice parameter per atomic percent lithium ($\partial a/\partial c_{\mathrm{Li}}$) in nm units in the aluminum-rich fcc solid solution (fcc-Al) and the $B32$ phase and the change of the bulk modulus per atomic percent lithium ($\partial B/\partial c_{\mathrm{Li}}$) in GPa units in the fcc-Al phase from CVM computations (this work) and as reported in Refs. 50–53. The misfit parameter δ, in percent, given by Eq. (28), between the fcc-Al phase and the Al_3Li-$L1_2$ precipitates, from lattice parameters computed with the CVM (no relaxation) at 300 and 500 K, and as observed (Refs. 49 and 54).

Property	Phase	This work	Experiment	Reference
$\partial a/\partial c_{\mathrm{Li}}$	fcc-Al	−0.000 051	−0.000 029	50
			−0.000 044	52
			−0.000 069	53
$\partial a/\partial c_{\mathrm{Li}}$	$B32$	−0.000 22	−0.000 25	50
			−0.000 34	51
δ (300 K)	fcc-Al/Al_3Li-$L1_2$	−0.28	−0.08	49
			−0.09	54
δ (500 K)	fcc-Al/Al_3Li-$L1_2$	−0.19		
$\partial B/\partial c_{\mathrm{Li}}$	fcc-Al	−0.48	−0.576	44

crease with increasing lithium content. Assuming isotropic elastic behavior and a constant Poisson ratio, one would expect that the bulk modulus would follow a similar trend, but this is not the case. Recent measurements[44] indicate that the bulk modulus decreases about 0.576 GPa per atomic percent lithium in solid solution, which corresponds remarkably well with our first-principles calculations which yield a decline of 0.48 GPa per atomic percent Li (Table IV). In addition, our calculations show that the bulk modulus reduction is virtually temperature independent. An interesting observation is that in order to account for an increase of the Young's modulus of 1.24 GPa per atomic percent Li,[44] and a decrease of the bulk modulus of 0.576 GPa per atomic percent Li, the Poisson ratio has to decrease rapidly from about 0.346 for pure aluminum to about 0.285 for an alloy with 14 at. % Li (maximum solubility), assuming isotropy. Glazer and Morris[45] observed such a decrease of the Poisson ratio with Li content, although their results have some quantitative ambiguity. The strong variation of the Poisson ratio suggests that Al-Li alloys will become increasingly anisotropic when the lithium content is raised. Contrary to results of our computations and experimental evidence,[44] Masuda-Jindo and Terakura[58] report an increase of the bulk modulus with lithium content in a recent augmented spherical wave (ASW) study of aluminum-rich Al-Li alloys. From a theoretical point of view, the ASW is less accurate than the FLAPW because the former assumes spherically averaged crystal potentials and charge densities. Also, within the ASW approach the volume of the crystal has to be filled by overlapping spheres. The radii of these atomic spheres for cases of more than one atom are adjustable parameters which have to be chosen. Furthermore, the number of four basis functions for the Li sphere corresponding to a maximum one-quantum number of 1 is quite small. We suspect that parameters chosen by Ref. 58 were not the most suitable ones for describing properly the anisotropy of the Al-Li interactions to get correct results for the bulk modulus. Finally, the ASW results would predict a hypothetical Al_7Li phase to be stable between the fcc Al-rich solid solution and the Al_3Li-$L1_2$ phases, a situation that has never been observed in experiment. We suspect that the listed ASW formation energy of Al_7Li is too low by a factor of 2 (Table 1 in Ref. 58). By contrast, the FLAPW results correctly describe the Al_7Li phase to be unstable with respect to the fcc-AL and $L1_2$-Al_3Li phases. The hypothetical Al_7Li phase has never been observed in actual Al-Li alloys.

Our first-principles method also enables us to predict whether Al_3Li-$L1_2$ precipitation will alter the bulk modulus. Assuming that an originally homogeneous Al-Li alloy with 9 at. % Li will form precipitates with 24 at. % Li and a solid solution with 5 at. % Li, we predict that the bulk modulus will increase upon ordering by about 0.23 GPa assuming uniform strain, and by about 0.08 GPa assuming uniform stress (see Ref. 59 for equations). A study by Broussard and Thomas[59] suggests that the Young's modulus increases by 0.6–1.3 GPa upon precipitation in alloys with 9 at. % Li. Another study[60] reports an increase of 0.1 GPa per volume percent of precipitate formed in alloys with low fractions of precipitate. The 9 at. % alloy could attain (in principle) a precipitate fraction of 21%, which would correspond to an increase of 2.1 GPa. Extrapolating the experimental results as is done here is likely to lead to inaccurate numbers, but at any rate it appears that our calculations can predict the fact that precipitation increases the bulk modulus of the alloy.

IV. SUMMARY AND CONCLUSION

A convenient way to introduce volume-dependent cluster interactions in the CVM has been presented and applied. A simple model for relaxation has been described that does not contain any fitting parameters and has the molar volumes and bulk moduli as sole input. Relaxation energy contributions thus calculated were shown to have a mild influence at the Li-rich side of the phase diagram and were virtually absent at the Al-rich side of the diagram.

The first-principles-based computation of the solid-state equilibria in the Al-Li system is, on many salient points, in agreement with experimental findings, such as (1) the correct prediction that fcc Al is much more stable than bcc Al; (2) the fcc structure is more stable than the bcc structure for Li at absolute zero temperature, and the small difference in the lattice stability of those two structures; (3) the $B32$ structure is much more stable than the $B2$ and $L1_0$ structures for the equiatomic alloy; (4) the fact that the free energy of the Al_3Li-$L1_2$ phase is only just above the common tangent between the Al-rich solid solution and the $B32$ phase at ambient temperatures, which indicates the metastability of the Al_3Li-$L1_2$ phase; (5) the prediction of the correct order of magnitude of the transition temperature of the metastable Al_3Li-$L1_2$ phase; (6) the relatively high solubility of Li in fcc Al, which increases with temperature, and the very small solubility of Al in both fcc and bcc Li; (7) the AlLi phase ($B32$) being so stable that it melts before disordering takes place; (8) the prediction that excess lithium causes an increase of the $B32$ lattice parameter and that lithium slightly decreases the lattice parameter of the Al-rich solid solution; (9) the decrease of the bulk modulus of the Al-rich solid solution with increasing Li content; and (10) the small negative value of the misfit between the Al-rich solid solution and the Al_3Li-$L1_2$ phase.

When empirical data was added, such as a simple concentration-dependent vibrational entropy and a regular solution free energy for the liquid, more correspondences with the experimental phase diagram were observed, such as (11) the prediction of eutectics at both the Al- and Li-rich sides of the phase diagram; the difference between the theoretical and experimental eutectic temperatures was attributed to the form of the free-energy expression for the liquid; (12) the $B32$ phase was computed to melt congruently, and a peritectic was calculated at about 70 at. % Li, between the eutectic at the Li-rich side and the melting point of the $B32$ phase.

A minor shortcoming was that the solid solubility of Li

in the Al-rich solid solution was computed to be larger than experimentally observed. Because of our choice to treat phase equilibria in the Al-Li system as a competition of ordering on fcc and bcc lattices (with first-, and first- and second-neighbor interactions only), the complex Al_4Li_9 ($mC26, B2/m$) and Al_2Li_3 ($hR5, R3m$) phases (see Ref. 15) could not be included in this study. It must be noted, however, that all phases that were included in this study, that is, fcc and bcc plus superstructures, had lattice stabilities that agreed with experimental observations. Furthermore, each phase appeared, at least qualitatively, to be correctly located in the phase diagram.

Although a practical first-principles formalism of the vibrational entropy is still lacking, first-principles studies of phase equilibria in the solid state have been shown to be feasible and useful.

ACKNOWLEDGMENTS

One of the authors (M.S.) wishes to thank Luc Wille, Jeff Hoyt, and Joe Kulik for helpful discussions and Mark Kraitchman for providing references regarding experimental work done on the Al-Li system. R.P. acknowledges the support of the Austrian Ministry of Science (Project No. 49.554/3-24/87). The research at the University of California was funded by the Air Force Wright Aeronautics Laboratory, administered through Los Alamos National Laboratory. Research at Northwestern University was supported by the National Science Foundation (NSF) (Grant No. DMR 85-18607 and by a grant from its Division of Advanced Computing at the Pittsburgh Supercomputer Center) and by the Air Force Office of Scientific Research (Grant No. 85-0358).

---

*Present address: Lawrence Livermore Laboratory, Livermore, California 94550.

†Present address: Institute for Physical Chemistry, University of Vienna, Waehringerstrasse 42, A-1090 Vienna, Austria.

[1]M. L. Saboungi and C. C. Husi, Comput. Coupl. Phase Diagr. Thermochem. (CALPHAD) **1**, 237 (1977).

[2]F. W. Gayle and J. B. van der Sande, Bull. Alloy Phase Diagrams **5**, 19 (1984).

[3]R. P. Elliott and F. A. Shunk, Bull. Alloy Phase Diagrams **2**, 353 (1981).

[4]A. J. McAlister, Bull. Alloy Phase Diagrams **3**, 177 (1982), and references therein.

[5]C. Sigli and J. M. Sanchez, Acta Metall. **34**, 1021 (1986).

[6]A. G. Khachaturyan, T. F. Lindsey, and J. W. Morris, Jr., Met. Trans. A **19**, 249 (1988).

[7]H. L. Skriver, Phys. Rev. B **31**, 1909 (1985); V. L. Moruzzi, J. F. Janak, and A. R. Williams, *Calculated Electronic Properties of Metals* (Pergamon, New York, 1978).

[8]W. Kohn and L. J. Sham, Phys. Rev. **140**, A1133 (1965); P. Hohenberg and W. Kohn, *ibid.* **136**, B864 (1964); M. Schlüter and L. J. Sham, Phys. Today **35**, 36 (1982).

[9]P. Turchi, M. Sluiter, and D. de Fontaine, Phys. Rev. B **36**, 3161 (1987); M. Sluiter, P. Turchi, Fu Zezhong, and D. de Fontaine, Phys. Rev. Lett. **60**, 716 (1988); C. Sigli, M. Kosugi, and J. M. Sanchez, Phys. Rev. Lett. **57**, 253 (1986).

[10]K. Terakura, T. Oguchi, T. Mohri, and K. Watanabe, Phys. Rev. B **35**, 2169 (1987); T. Mohri, K. Terakura, T. Oguchi, and K. Watanabe, Acta Metall. **36**, 547 (1988).

[11]H. J. F. Jansen and A. J. Freeman, Phys. Rev. B **30**, 561 (1984).

[12]J. W. Connolly and A. R. Williams, Phys. Rev. B **27**, 5169 (1983).

[13]L. G. Ferreira, A. A. Mbaye, and A. Zunger, Phys. Rev. B **35**, 6475 (1987); A. A. Mbaye, L. G. Ferreira, and A. Zunger, Phys. Rev. Lett. **58**, 49 (1987).

[14]M. Sluiter and P. Turchi, in *Alloy Phase Stability*, Vol. 163 of *NATO Advanced Study Institute, Series, E*, edited by G. M. Stocks and A. Gonis (Plenum, New York, 1989), p. 521; M. Sluiter and P. E. A. Turchi, Phys. Rev. B **40**, 11 215 (1989).

[15]J. M. Sanchez and C. H. Lin, Phys. Rev. B **30**, 1448 (1984).

[16]P. Villars and L. D. Calvert, *Pearson's Handbook of Crytallographic Data for Intermetallic Phases* (American Society of Metals, Metals Park, OH, 1985).

[17]M. Sluiter, R. Podloucky, X. Q. Guo, and A. J. Freeman (unpublished).

[18]R. Podloucky, H. J. F. Jansen, X. Q. Guo, and A. J. Freeman, Phys. Rev. B **37**, 5478 (1988).

[19]L. Hedin and B. I. Lundqvist, J. Phys. C **4**, 2064 (1971).

[20]G. Lehmann and M. Taut, Phys. Status Solidi **54**, 469 (1972).

[21]J. M. Sanchez, F. Ducastelle, and D. Gratias, Physica (Amsterdam) **128A**, 334 (1984); A. Finel, Thèse de Doctorat d'Etat, Université Pierre et Marie Curie, Paris, 1987 (unpublished).

[22]J. M. Sanchez and D. de Fontaine, Phys. Rev. B **17**, 2926 (1978); T. Mohri, J. M. Sanchez, and D. de Fontaine, Acta Metall. **33**, 1171 (1985).

[23]J. M. Sanchez and D. de Fontaine, Phys. Rev. B **21**, 216 (1980).

[24]J. A. Barker, Proc. R. Soc. London, Ser. A **216**, 45 (1953); J. Hijmans and T. de Boer, Physica (Utrecht) **21**, 471 (1955); **21**, 485 (1955); **22**, 408 (1956).

[25]R. Kikuchi, Phys. Rev. **81**, 988 (1951).

[26]R. Kikuchi, J. Chem. Phys. **60**, 1071 (1974).

[27]D. de Fontaine, in *Solid State Physics*, edited by F. Seitz, D. Turnbull, and H. Ehrenreich (Academic, New York, 1979), Vol. 34, p. 73; J. M. Sanchez, D. de Fontaine, and W. Teitler, Phys. Rev. B **26**, 1465 (1982).

[28]J. M. Sanchez and D. de Fontaine, Phys. Rev. B **25**, 1759 (1982).

[29]L. S. Darken and R. W. Gurry, *Physical Chemistry of Metals* (McGraw-Hill, New York, 1953); W. Hume-Rothery, R. E. Smallman, and C. W. Haworth, *Structure of Metals and Alloys*, 5th ed. (Institute of Metals, London, 1969); W. B. Pearson, *The Crystal Chemistry and Physics of Metals and Alloys* (Wiley, New York, 1972); O. Kubaschsewki, in *Phase Stability of Metals and Alloys*, edited by P. Rudman, J. Stringer, and R. I. Jaffe (McGraw-Hill, New York, 1967).

[30]H. G. Smith, Phys. Rev. Lett. **58**, 1228 (1987).

[31]C. S. Barrett and O. R. Trautz, Trans. AIME **175**, 579 (1948); C. S. Barrett, Acta Crystallogr. **9**, 671 (1956).

[32]C. S. Barrett, Phys. Rev. **72**, 245 (1947).

[33]G. Moraitis and F. Gautier, J. Phys. F **7**, 1421 (1977); **7**, 1841 (1977); **8**, 1653 (1978); H. Bakker, Phys. Status Solidi B **109**, 211 (1982); A. A. H. J. Waegmaekers and H. Bakker, in *Phase Transformations in Solids*, Vol. 21 of *Material Research Society Symposium Proceedings*, edited by T. Tsakalakos

(North-Holland, New York, 1984), p. 343.
[34]P. J. Wojtowicz and J. G. Kirkwood, J. Chem. Phys. **33**, 1299 (1960).
[35]L. Kaufman and H. Bernstein, *Computer Calculation of Phase Diagrams* (Academic, New York, 1970), p. 185.
[36]J. Friedel, J. Phys. (Paris) Lett. **35**, L59 (1974).
[37]J. L. Barrat, M. Baus, and J. P. Hanse, Phys. Rev. Lett. **56**, 1063 (1986); S. J. Smithline and A. D. J. Haymet, J. Chem. Phys. **86**, 6486 (1987); A. D. J. Haymet, Science **236**, 1076 (1987).
[38]L. F. Mondolfo, *Aluminum Alloys: Structure and Properties* (Butterworths, New York, 1979), pp. 82 and 308.
[39]R. Hultgren *et al.*, *Selected Values of the Thermodynamic Properties of the Elements* (American Society of Metals, Metals Park, OH, 1973), pp. 25 and 281.
[40]E. A. Brandes, *Smithells Metals Reference Book,* 6th ed. (Butterworths, Boston, MA, 1983).
[41]T. L. Hill, *An Introduction to Statistical Thermodynamics,* 2nd ed. (Addison-Wesley, Reading, MA, 1962), p. 78.
[42]A. P. Miodownik, in *Computer Modeling of Phase Diagrams,* edited by L. H. Bennett (AIME, Warrendale, PA, 1986), p. 253.
[43]V. L. Moruzzi, J. F. Janak, and K. Schwarz, Phys. Rev. B **37**, 790 (1988).
[44]W. Mueller, E. Bubeck, and V. Gerold, in *Proceedings of the 3rd International Conference on Aluminum-Lithium Alloys,* edited by C. Baker, P. J. Gregson, S. J. Harris, and C. J. Peel (TMS-AIME, London, 1986), p. 435.
[45]J. Glazer and J. W. Morris, AIAA J. **25**, 1271 (1987).
[46]D. de Fontaine, Acta Metall. **23**, 553 (1975).
[47]V. Radmilovic, A. G. Fox, and G. Thomas, Acta Metall. **37**, 2385 (1989).
[48]M. Tamura, T. Mori, and T. Nakamura, J. Jpn. Inst. Met. **34**, 919 (1970).
[49]D. B. Williams and J. W. Edington, Met. Sci. **9**, 529 (1975).
[50]E. D. Levine and E. J. Rapperport, Trans. AIME **227**, 1204 (1963).
[51]K. Kishio and J. O. Brittain, J. Phys. Chem. Solids **40**, 933 (1979).
[52]H. J. Axon and W. Hume-Rothery, Proc. R. Soc. London, Ser. **A193**, 1 (1948).
[53]S. H. Kellington, D. Loveridge, and J. M. Titman, Br. J. Appl. Phys. (J. Phys. D) **2**, 1162 (1969).
[54]S. F. Baumann and D. B. Williams, in *Proceedings of the 2nd International Conference on Aluminum-Lithium Alloys,* edited by T. H. Sanders, Jr. and E. A. Starke, Jr. (TMS-AIME, Warrendale, PA, 1986), p. 17.
[55]B. Noble, S. J. Harris, and K. Dinsdale, J. Mater. Sci. **17**, 461 (1982).
[56]E. Agyekum, W. Kuch, E. A. Starke, Jr., S. C. Jha, and T. H. Sanders, Jr., in Ref. 44, p. 448.
[57]J. Glazer (private communication).
[58]K. I. Masuda-Jindo and K. Terakura, ISSP Report No. A 2011, 1988 (unpublished); Phys. Rev. B **39**, 7509 (1989).
[59]F. Broussard and M. Thomas, in Ref. 44, p. 442.
[60]M. E. O'Dowd, W. Ruch, and E. A. Starke, Jr., J. Phys. (Paris) Colloq. **48**, C3-565 (1987).